A simple approach to multi degree-of-freedom loading in a geotechnical centrifuge

Manuscript accepted to *ASTM Geotechnical Testing Journal* on 11/07/2018

Conleth D. O'LOUGHLIN
Centre for Offshore Foundation Systems – M053,
A node of ARC Centre for Geotechnical Science and Engineering
University of Western Australia
35 Stirling Highway, Crawley, Perth, WA 6009, Australia
Tel: +61 8 64887326
Email: conleth.oloughlin@uwa.edu.au
Michael L. COCJIN
Centre for Offshore Foundation Systems
A node of ARC Centre for Geotechnical Science and Engineering
Email: michael.cocjin@research.uwa.edu.au
Susan M. GOURVENEC
Centre for Offshore Foundation Systems, UWA
A node of the ARC Centre for Geotechnical Science and Engineering
Email: susan.gourvenec@uwa.edu.au

Sam A. STANIER

Centre for Offshore Foundation Systems, UWA
A node of the ARC Centre for Geotechnical Science and Engineering
Email: sam.stanier@uwa.edu.au

No. of words: **4,102** (excluding ABSTRACT, including Sections 1 – 6)

No. of tables: **0**

No. of figures: **11**

ABSTRACT

This paper considers an alternative approach for multi-planar loading and multi degree-of-freedom movement in geotechnical centrifuge model tests. The multi degree-of-freedom loading system allows for vertical load control on the vertical axis, and either displacement or load control on the two horizontal axes, whilst allowing rotation about these axes. The system is described in detail and the system performance is validated through results from a centrifuge test comparing observed results with analytical and numerical solutions. The validation of the system considers a mudmat foundation under large amplitude lateral displacement, where two displacement degrees-of-freedom and two rotational degrees-of-freedom were of interest. However, the apparatus is versatile and can be used for testing other foundation types or pipelines, with up to six degrees-of-freedom.

1. INTRODUCTION

Offshore structures are typically subjected to multi-directional loading and respond with displacement in multiple degrees of freedom. Foundations of fixed-base structures, oil and gas platforms or wind turbines, experience a combination of vertical load from the self-weight of the structure, horizontal loads from the action of wind, waves and currents, and moment loading from the height offset between the action of the horizontal loads and the foundation; foundations of subsea structures can experience complex multi-directional loading from multiple pipeline and spool expansion loads acting at vertical and horizontal eccentricities to the centroid of the foundation (Randolph 2012, Feng et al. 2014); offshore pipelines are subject to vertical self-weight loads, multi-directional installation loads and thermally induced axial and lateral loads during operation and respond with settlement/burial, axial walking and lateral buckling.

Independent control of loading and acquisition of displacement, or vice versa, in all six degrees of freedom poses quite an experimental challenge for actuation systems. This is more achievable at 1***g*** than in a centrifuge as the space requirements for the actuation and position measurement systems can be more easily accommodated on the laboratory floor than within the constrained space available on a centrifuge package (Byrne 2014). Centrifuge actuators typically have two or three displacement degrees of freedom (DoF) along the horizontal and vertical planes, although actuation systems that add a rotational DoF have also been developed (Dean et al. 1997, Punrattanasin et al., 2003, Cocjin and Kusakabe 2013, Kong 2012, Zhang et al. 2013, Gaudicheau et al. 2014). To the authors' knowledge a six DoF actuation system has not yet been developed for use in a geotechnical centrifuge.

Independent control of loads or displacement in all degrees of freedom is not a necessity for many practical applications involving multi-directional loading and resulting displacements. A practical approach to multi DoF actuation in a geotechnical centrifuge may, in many cases, be to use existing actuators to control displacements or loads along the principal axes, whilst permitting rotational degrees of freedom about the same axes. This paper describes such an approach, firstly describing a new multi-DoF loading system, before assessing the system performance as measured in a centrifuge mudmat test on normally consolidated kaolin clay.

2. DESIGN OF THE MULTI-DoF LOADING SYSTEM

2.1 General arrangement

The general arrangement of the new multi-DoF loading system, actuator and model is illustrated in **Figure 1**.

The multi-DOF loading system (item [1] in **Figure 1**) enables movement in four DoF under vertical load control and with either horizontal load or displacement control. As shown by **Figures 1(a-b)**, it is designed to be operated in conjunction with an actuator[2] that provides motion in the vertical and horizontal directions. The actuator is mounted on top of a strongbox containing the soil model. The main part of the multi-DoF loading system is a “C-shaped loading arm” (described in detail in the following section) that connects to the actuator by way of a solid aluminium shaft secured at the collar connection[6] of the actuator’s vertical axis. Two rotational DoF are allowed for within the C-shaped loading arm, which together with the two translational DoF provided by the horizontal and vertical axes of the actuator, comprise the four DoF allowed on the model infrastructure. This is shown by **Figure 2**, which also defines the positive sign convention for the loads and displacements, and the reference point (RP) where the loads and displacements are defined on a rectangular foundation.

The multi-DoF loading system was developed for and trialled on a model pipeline end termination mudmat, where displacement along the longitudinal and vertical axes, and rotation about the two orthogonal horizontal axes were of interest (i.e. four DoF). However, the use of an actuator with a second horizontal axis and an additional rotational degree of freedom within the C-shaped arm would enable load or displacement control in three DoF and movement in all six DoF (without control in the rotational DoF).

The multi-DoF loading system can be operated in either load or displacement control on the horizontal axis and on load control on the vertical axis. Motion along these actuator axes is provided by DC servo-motors that drive vertical and horizontal lead screws[7,8] (**Figure 1(b)**). The actuator axes are controlled by the UWA Package Actuator Control System (PACS) (De Catania et al., 2010), an in-house software written in Labview. This software runs on an in-flight computer mounted on the centrifuge and acts as a slave to a master computer in the centrifuge control room, with communication via an Ethernet link across an optical slip ring. The control software is operated via a remote desktop linked to the in-flight computer.

Load- or displacement-controlled operation of the actuator can be achieved with a software feedback loop using the outputs of a load cell[11,12] or a displacement transducer[4,5]. The software can also automate loading or displacement sequences through its waveform generator. The waveform can be generated for monotonic loading or displacement sequences using a ramp function, or cyclic loading or displacement sequences using a sine, square, triangle or sawtooth function (De Catania et al. 2010).

2.2 Loading arm description

As described above, the C-shaped loading arm provides the rotational DoF. Details of the loading arm are provided in **Figures 1(c-d)**. The upper C section is fabricated from aluminium and is 235 mm long along the y axis, with provision for a bolted connection to the aluminium shaft attached to the actuator. An eyelet[17] is provided at the free end of the upper C section to append the vertically-suspended load cell[11], whilst the other end is bolted to a vertical shaft forming the middle C section. The shaft for the middle C section is fabricated from stainless steel, 105 mm long with 25 mm diameter, and is attached to the lower C section by a hinge. The lower C section is comprised of an S-shaped load cell[12], an in-line stainless steel cylindrical roller bearing[14] and a 100 mm long aluminium section with a hinge[15] at its free end. The roller bearing provides the rotational DoF about the y axis, whereas the hinge at the end of the aluminium section provides the connection to the foundation model and the rotational DoF about the x axis. An eyelet[16], located directly above this hinge, connects to the vertically-suspended load cell[11] via wire cable and polyethylene line (to eliminate rigidity), completing the connection between the upper and lower C sections. The height of the hinge[15] from the base of the attached model foundation is adjustable depending on the test requirements.

2.3 System instrumentation

A vertically-suspended load cell[11] with a measurement range of 1.4 kN is suspended in-line between the eyelets[17,16] on the upper and lower C sections. The load cell was connected to the upper eyelet[17] using steel cable, but to the lower eyelet[16] using the polyethylene line, to ensure that the link between the two eyelets could only be in tension. This was a design requirement as this load cell measures the combined self-weight of the lower C section and the attached model foundation when not in contact with the soil surface. The submerged weight of the foundation, V, and hence the on-bottom pressure applied to the soil, can then be controlled by operating the vertical axis of the actuator under load control using the analogue feedback from the vertical load cell. The S-shaped axial load cell[12] on the lower C section has a measurement range of 150 N and measures the horizontal load, H, along the y axis.

Displacements along the y and z axes are measured using the optical encoders located on the vertical and horizontal axes of the actuator. A laser displacement sensor[5] (Keyence®, model LB-70-11) with a measurement range of 80 mm is located on a bracket connected to the actuator and oriented towards a target[18] at the junction of the middle and lower C sections of the loading arm (**Figure 1(c)**). This provides an additional measurement of the foundation displacement along the y axis, independent of that determined from the optical encoder on the actuator's horizontal axis.

Four additional laser displacement sensors[4] with a measurement range of 80 mm measure the vertical displacement at each corner of the foundation, although these measurement locations can be adjusted if required. These displacement sensors are mounted directly above the model foundation on a steel plate that is fixed to the actuator, such that the sensors move horizontally in unison with the actuator and hence the model foundation (**Figure 1(b)**). Independent measurement of these corner vertical displacements allows the rotation about the x and y axes – θ_{xx} and θ_{yy} respectively – to be determined.

3. SUMMARY OF CENTRIFUGE TEST USED TO ILLUSTRATE LOADING SYSTEM CAPABILITY

System performance of the multi-DoF loading system is assessed in the next section using the results from a centrifuge test that was conducted to investigate the load and displacement response of a pipeline end termination mudmat foundation on normally consolidated clay when subjected to cycles of large-amplitude lateral movements under low vertical load, simulating the expansion associated with start-up and shut-down operations of an offshore pipeline. Testing was conducted in the UWA beam centrifuge. A complete description of this centrifuge, as commissioned in 1989, is provided by Randolph et al. (1991). The centrifuge test results are reported in model scale, unless stated otherwise, in order to demonstrate the accuracy of the new loading system.

3.1 Soil model

A normally consolidated kaolin clay sample was prepared from slurry at twice the liquid limit and consolidated under self-weight in the centrifuge at 100g for 3.5 days. After consolidation was essentially complete, the centrifuge was stopped and a minimum amount of clay was scraped from the sample to create a level surface.

The final sample dimensions were 650 mm by 390 mm in plan with a height of 130 mm. A miniature T-bar penetrometer (Stewart & Randolph, 1991) with a projected (penetrating) area of 100 mm^2 was used to determine the depth profile of undrained shear strength, s_u. The T-bar was penetrated into the soil at a rate of 1 mm/s to ensure undrained conditions (Randolph & Hope, 2004) and s_u was determined from the measured penetration resistance using a constant T-bar factor of 10.5 (Martin & Randolph, 2006). **Figure 3** shows the s_u profile with depth, which can be well described by $s_u = 0.53 + 0.86z$ (kPa), where z is the penetration depth in prototype scale (m). The average effective unit weight of the soil, $\gamma'_{avg} = 5.7$ kN/m^3 was assessed from moisture content measurements made on a core sample taken after testing, giving a normally consolidated strength ratio of $(s_u/\sigma'_{v0})_{\text{NC}} \sim 0.15$, similar to that determined from other recent centrifuge studies on UWA kaolin (Chow et al. 2014; Hu et al. 2014; Morton et al. 2014).

3.2 Model foundation

A rectangular mudmat foundation, with aspect ratio $B/L = 0.5$, was used in the centrifuge test. **Figure 4** shows a schematic of this model foundation attached to the loading arm, showing profile views in (a) y-z, and (b) x-z planes. The foundation has underside base plate dimensions, $B = 50$ mm and $L = 100$ mm (giving a basal area of $A = 5000$ mm^2), and a height of 5 mm (equivalent to prototype plan dimensions of 5 m by 10 m and height of 0.5 m). The model foundation was fabricated with an edge ‘ski’ (inclined at 30°) along each side. The purpose of the ski was to reduce foundation tipping (overturning) and encourage sliding.

The mudmat was fabricated from acetal (polyoxymethylene (POM)) that has a density of 1410 kg/m^3, which is sufficiently low to allow a model mudmat of solid section to replicate the self-weight of a field mudmat, typically manufactured from steel but not solid in section. With the current modelling approach, as described earlier, adjustment to a targeted submerged on-bottom weight is achieved using load control on the vertical axis of the actuator. This capability means that scaling of the submerged weight of the prototype foundation is not a modelling requirement, although was achieved in this case. Acetal has a Young’s modulus and Poisson ratio of 3.1 GPa and 0.39 respectively, sufficiently stiff to be considered as rigid relative to the soft clay. Fine silica sand was glued to the base plate as a rough foundation–soil interface was of interest for these tests. The faces of the edge ‘ski’ retained a smooth finish.

Circular discs propped on slender posts were located at each corner of the model foundation to serve as targets for the vertically-orientated laser displacement sensors. The height of the posts can be adjusted to keep the circular discs above the water surface during the test to avoid refraction of the laser beam in the water.

Figure 5 shows the DoF for the model foundation with the currently configured loading system and the two-directional actuator. Vertical displacement of the model foundation along the z axis is quantified either through the displacement of the actuator's vertical axis, $w_{(encoder)}$ or through the average of the corner vertical laser displacements, $w_{(laser)}$ (**Figure 5(a)**). Horizontal displacement of the model foundation along the y axis may be taken either as the displacement of the actuator's horizontal axis, $u_{y(encoder)}$ or from the independent laser displacement sensor measurement, $u_{y(laser)}$ (**Figure 5(b)**). Rotation of the model foundation about the x and y axes – θ_{xx} and θ_{yy} respectively – may be quantified from the difference of corner vertical laser displacement measurements (**Figures 5(c-d)**). Whilst the current system configuration enables foundation displacement in four DoF, displacement-control is limited to horizontal y axis.

3.3 Loading program

As described earlier, the four DoF loading system is operated with the vertical axis of the actuator under load control and the horizontal axis of the actuator under either displacement or load control. The test presented here to illustrate the performance of the apparatus employed displacement control for the horizontal axis. The time history of imposed loads and displacements are shown in **Figure 6**: vertical load, V (**Figure 6(a)**) and horizontal displacement, u_y (**Figure 6(b)**).

Phase 1 of the test involved foundation touchdown and consolidation under the operative vertical load, V_{op}. Foundation touchdown can be performed under either displacement or load control. In this test, displacement control was used with the vertical axis of the actuator displaced positively – initially at a velocity of 0.1 mm/s, reducing to 0.01 mm/s as the foundation approached the mudline – until about one third of the targeted load was observed, at which point the vertical axis of the actuator was switched into load-control mode and a target load of V_{op} specified. This process was automated using the PACS software, with manual fine adjustment of the load control as required. A consolidation period of approximately 4 hours (4.5 years in prototype scale) was allowed after touchdown of the mudmat to bring the soil beneath the foundation sufficiently close to a fully consolidated state at the end of the installation phase. During Phase 1 (including the consolidation stage), settlement along the z axis, and rotation about the x and y axes were permitted, but horizontal displacement along the y axis was not allowed.

Phase 2 involved undrained large amplitude cyclic sliding of the mudmat foundation. As in Phase 1, the actuator motion was automated using the waveform generator in the PACS software. The sliding cycles are as defined in **Figure 6(b)** and comprise a forward slide equal to half the breadth of the foundation $u_{y(max)} = 0.5B$, a long interim pause during which $\Delta u_y = 0$, a backward slide until $u_y = 0$, and finally a short interim pause during which $\Delta u_y = 0$. The horizontal displacement was carried out at a velocity of 1.0 mm/s. This gives a one-way sliding duration of 25 s (< 3 days in prototype scale), sufficiently short for any significant dissipation of excess pore water in the soil beneath the foundation to occur during sliding (Cocjin et al. 2014). The test involved $N = 40$ loading cycles, with each loading cycle comprising a forward slide, long period of consolidation, backward slide and short period of consolidation. The long interim pause permitted after each forward slide represents the period when a pipeline is in operation between scheduled shutdowns, with shutdowns typically occurring a few times a year. As such the reconsolidation episode at $u_y = u_{y(max)}$ was 13 minutes, equivalent to 3 months in prototype scale. The short interim pause permitted after each backward slide simulates the brief shutdown period after the pipe cools and contracts and the foundation has returned to its installation position, $u_y = 0$. Shutdowns are typically less than a day, modelled in the centrifuge test as 8 s. During Phase 2, settlement along the *z* axis, and rotation about the *x* and *y* axes were permitted, with horizontal displacement along the *y* axis allowed only during the forward and backward slides but locked during the interim pauses.

An operative vertical load, V_{op} corresponding to ~ 30% of the unconsolidated, undrained vertical capacity of the mudmat foundation, was selected as a realistic field value, and to allow for a pure sliding mechanism in response to horizontal loading under undrained conditions (Green, 1954; Gourvenec & Randolph, 2003; Cathie *et al.*, 2008).

4. TECHNICAL PERFORMANCE OF THE MULTI-DOF LOADING SYSTEM

The technical performance of the multi DoF loading system is examined in this section by considering the load and displacement response of the model foundation during the test. **Figure 7** shows a time history of the vertical load, *V*; horizontal displacement, $u_{y(encoder)}$ (i.e. taken as the horizontal displacement of the actuator); horizontal load, *H*; vertical displacement, $w_{(laser)}$ (i.e. taken as the average of the vertical displacements at the foundation corners); and foundation rotation about the *x* and *y* axes – θ_{xx} and θ_{yy} respectively. The data are provided in **Figure 7(a**) through to **Figure 7(e)** for vertical touchdown of the foundation, **Figure 7(f)** through to **Figure 7(j)** for post-installation consolidation and the first 15 undrained sliding cycles, and **Figure 7(k)** through to **Figure 7(o)** for the first sliding and re-consolidation cycle.

It is clear from **Figure 7** that the system is capable of enabling and measuring required foundation movements in four DoF; displacements develop along the *y* and *z* axes, and rotations develop about the *x* and *y* axes.

Displacement along the z axis, $w_{(laser)}$, is continuous during the test as this axis is operated in load control, whereas displacement only occurs along the y axis, $u_{y(encoder)}$ during the forward and backward slides. The change in z axis displacement, i.e. settlement, Δw, is positive during the post-touchdown consolidation, cycles of re-consolidation and during forward slides, but negative during backward slides. As the foundation is free to rotate about the x and y axes, θ_{xx} and θ_{yy} are non-zero throughout the test, and change most rapidly during the undrained sliding cycles.

Vertical load develops from time, t = -240 s to t = 0 as the foundation is gradually lowered to the soil surface under displacement control, initially at a displacement rate of 0.1 mm/s (to t = -167 s) and then 0.01 mm/s. From t = 0 the vertical axis was under load control, with the achieved load in the range V_{op} = 10 ± 0.35 N during the consolidation phase when $\Delta u_y = 0$, and V_{op} = 10 ± 1.5 N during the undrained sliding cycles when $\Delta u_y \neq 0$. The higher variation in the achieved load is partly due to the difficulty in selecting PID (proportional–integral–derivative) controller parameters that work effectively during static and non-static conditions, although mechanical slack between the leadscrew and the nut on the actuator axes can also deteriorate the quality of the load control. **Figure 8** shows the equivalent response measured in separate tests in which the actuator axes were adjusted mechanically to reduce backlash, where the variation in the maintained load during the undrained sliding cycles is reduced approximately threefold. However, it is worth noting that the maximum variation corresponds to 0.1 % of the measurement range of the load cell (1.4 kN) and that the variation would reduce if a load cell with a lower measurement range were used. The horizontal load, H is essentially zero during foundation touchdown and post-touchdown consolidation, which is to be expected as $u_y = 0$ during this time. During the undrained sliding cycles, H is positive during forward slides and negative during backward slides. H also increases with increasing loading cycles, reflecting the higher seabed strength brought about by the consolidation periods between sliding events.

Figure 9 compares the foundation displacements as assessed from the actuator motion with the independent laser displacement sensor measurements in: (a) vertical and (b) horizontal directions. The vertical displacement of the actuator, $w_{(encoder)}$, is typically no more than 0.2 mm lower than that determined from the average of the laser displacement sensors, $w_{(laser)}$, equivalent to less than 4% difference in the actual displacement. The horizontal displacement of the actuator $u_{y(encoder)}$ is initially close to the value measured by the horizontal laser displacement sensor, $u_{y(laser)}$. However, as the cycles progress, the difference between $u_{y(encoder)}$ and $u_{y(laser)}$ increases to a maximum deviation of 1.5 mm (6 %) due to a progressive increase in system compliance brought about by the increasing horizontal load, *H*, reflecting the strength increases in the clay. This reduced slide displacement was negligible for the current test, involving slide distances of 0.5*B*. In other scenarios it may be more appropriate to use the independent displacement measurement rather than the encoder as the displacement feedback for the actuator's horizontal axis.

5. EXAMPLE APPLICATION OF THE MULTI-DOF LOADING SYSTEM

The load and displacement response from the sliding mudmat foundation test is presented in **Figure 10**. **Figure 10(a)** shows (imposed) horizontal displacement against (observed) settlement over the 40 cycles of the test, and **Figure 10(b)** shows the cycle-by-cycle increase in horizontal sliding resistance against the (imposed) horizontal displacement. **Figures 10(c-d)** represent the measured displacement and load respectively, midway through the slide, i.e. at $u_y/B = 0.125$. Foundation rotations, θ_{xx} and θ_{yy} are provided in **Figure 10(e)**, showing that rotations are minimal.

An independent quantification of the foundation consolidation settlement was made by considering the difference in void ratio profiles with depth obtained within the foundation footprint and in free-field soil (e_0) from vertical core soil samples taken after the test (inset **Figure 11(a)**). The final consolidation settlement is calculated from the measured change in void ratio by

$$\sum w_{cons,f} = \int_{z=0}^{z\to\infty} \frac{\Delta e}{1+e_0} dz \tag{1}$$

and is seen to agree well with the final value of consolidation settlement Σw_{cons} determined from the laser displacement sensors as shown in **Figure 11(a)**.

The difference between the total observed settlement, Σw and the accumulated consolidated settlement, Σw_{cons} is a measure of the amount of soil that accumulates as berms on either side of the foundation during the sliding cycles, shown in **Figure 11(b)**.

The measured horizontal resistance, *H*, expressed as a coefficient of sliding friction, $\mu = H/V$, during the first slide and during the loading cycles is plotted against normalised foundation displacement, u_y/B in **Figure 12(a)** and **Figure 12(b)**, respectively. During the first slide, a peak resistance at low horizontal displacement is observed which then reduces with foundation displacement, reaching a steady state of $\mu = 0.15$ at $u_y/B \approx 0.15$. The steady state coefficient of sliding friction derived from the test observation agrees well with analytical and numerical predictions based on critical state soil mechanics (Cocjin et al. 2016; Feng & Gourvenec 2015).

Figure 12(c), which plots the mid-slide values of coefficient of sliding friction, μ against cycle number, N shows that a long term sliding resistance given by $\tan\varphi'$ where $\varphi' = 23.5°$ is the internal angle of soil friction, is eventually achieved when the soil has undergone sufficient cycles of sliding (and hence shearing), pore pressure generation and reconsolidation to reach critical state conditions, resulting in no further contraction and excess pore pressure generation (Cocjin et al. 2015, Cocjin et al. 2016, Feng & Gourvenec 2016).

6. CLOSING REMARKS

Multi degree-of-freedom loading in a geotechnical centrifuge environment is challenging, but necessary to understand the behaviour of geotechnical structures that experience combined loading. This paper has simplified the challenge somewhat by proposing a multi DoF loading system that uses a conventional two or three dimensional actuator to actuate along the principal axes, whilst using roller bearings to allow rotation about the same axes. Whilst the system does not permit for independent control of the rotational DoF, the simplicity and flexibility of the system is appealing and sufficient for simulating various boundary value problems involving multi-directional loading and freedom of movement. This has been demonstrated in this paper by simulating the whole-life cycle of a pipeline end termination mudmat under large amplitude lateral displacement. The loading arm apparatus could also be used to investigate the performance of other foundation systems or pipelines under selected modes of multi-directional loading.

7. ACKNOWLEDGEMENTS

This work forms part of the activities of the Centre for Offshore Foundation Systems (COFS), currently supported as a node of the Australian Research Council’s Centre of Excellence for Geotechnical Science and Engineering, and through the Fugro Chair in Geotechnics, the Lloyd’s Register Foundation Chair and Centre of Excellence in Offshore Foundations and the Shell EMI Chair in Offshore Engineering. The work presented in this paper is supported through ARC grant DP140100684. Development of the multi DoF loading system was supported through a contract with Fugro AG.

8. REFERENCES

Bienen B, Byrne BW, Houlsby GT and Cassidy MJ (2006) Investigating six-degree-of-freedom loading of shallow foundation on sand. *Géotechnique* **56(6)**: 367–379, http://dx.doi.org/10.1680/geot.2006.56.6.367.

Byrne BW (2014) Laboratory scale modelling for offshore geotechnical problems. In ICPMG2014 – Physical Modelling in Geotechnics: Proceedings of the 8th International Conference on Physical Modelling in Geotechnics (Gaudin C and White D (eds)). CRC Press, Boca Raton, FL, USA, pp. 61–75.

Cathie D, Morgan N, and Jaeck C (2008) Design of sliding foundations for subsea structures. In *Proc. BGA International Conference on Foundations*. Dundee, Scotland, pp. 24–27.

Cheng N, Gaudin C, Cassidy MJ and Bienen B (2014) Centrifuge study of the combined bearing capacity of a hybrid foundation system. In *Proceedings ICPMG2014 – Physical Modelling in Geotechnics: Proceedings of the 8th International Conference on Physical Modelling in Geotechnics* (Gaudin C and White D (eds)). CRC Press, Boca Raton, FL, USA, pp. 487–492.

Chow SH, O'Loughlin CD, and Randolph MF (2014) Soil strength estimation and pore pressure dissipation for free-fall piezocone in soft clay. *Géotechnique* **64(10)**: 817–827, http://dx.doi.org/10.1680/geot.14.P.107.

Cocjin M and Kusakabe O (2013) Centrifuge observations on combined loading of a strip footing on dense sand. *Géotechnique* **63(5)**: 427–433, http://dx.doi.org/10.1680/geot.11.P.075.

Cocjin M, Gourvenec S, White D, and Randolph M (2014) Tolerably mobile subsea foundations – observations of performance. *Géotechnique* **64(11)**: 895–909, http://dx.doi.org/10.1680/geot.14.P.098.

Cocjin M, Gourvenec S, White D, and Randolph M (2015) Effects of drainage on the response of a sliding subsea foundation. In *Proceedings of the 3rd international symposium on frontiers in offshore geotechnics (ISFOG 2015), Oslo, Norway* (ed. V. Meyer). CRC Press London, UK, pp. 777–782.

Cocjin M, Gourvenec S, White D, and Randolph M (2016) Theoretical framework for predicting the response of tolerably mobile subsea installations. Paper under review.

De Catania S, Breen J, Gaudin C, and White DJ (2010) Development of a multiple-axis actuator control system. In *Proceeding Int. Conf. on Phys. Modelling in Geotechnics '10, Zurich* (Springman S, Laue J and Seward L (eds)). Taylor & Francis Group, London, UK, pp. 325–330.

Dean ETR, James RG, Schofield AN and Tsukamoto Y (1997) Theoretical modelling of spudcan behaviour under combined load. *Soils and Foundations* **37(2)**: 1–15, http://dx.doi.org/10.3208/sandf.37.2_1.

Feng X and Gourvenec S (2016) Modelling sliding resistance of tolerably mobile subsea mudmats. *Géotechnique* **66(6)**: 490–499, http://dx.doi.org/10.1680/jgeot.15.P.178.

Feng X, and Gourvenec S (2015) Consolidated undrained load-carrying capacity of subsea mudmats under combined loading in six degrees of freedom. *Géotechnique* **65(7)**: 563 – 575, http://dx.doi.org/10.1680=geot.14.P.090.

Feng X, Randolph MF, Gourvenec S and Wallerand R (2014) Design approach for rectangular mudmats under fully three-dimensional loading. *Géotechnique* **64(1)**: 51–63, http://dx.doi.org/10.1680/geot.13.P.051.

Gaudicheau P, Thorel L, Néel A, Audrain Ph, Loozaadaand C, and Monroy J (2014) Improvement of the IFSTTAR robot control system. In *Proceedings ICPMG2014 – Physical Modelling in Geotechnics: Proceedings of the 8th International Conference on Physical Modelling in Geotechnics* (Gaudin C and White D (eds)). CRC Press, Boca Raton, FL, USA, pp. 221 – 226.

Gourvenec S, and Randolph MF (2003) Effect of strength non-homogeneity on the shape of failure envelopes for combined loading of strip and circular foundations on clay. *Géotechnique* **53(6)**: 575–586, http://dx.doi.org/10.1680/geot.2003.53.6.575.

Green AP (1954) The plastic yielding of metal junctions due to combined shear and pressure. *J. Mech. Phys. Solids* **2(3)**: 197–211.

Hu P, Stanier A, Cassidy MJ and Wang D (2014) Predicting peak resistance of spudcan penetrating sand overlying clay. *J. Geotech. Geoenviron. Eng.* 140(2): 01013009, http://dx.doi.org/10.1061/(ASCE)GT.1943-5606.0001016

Kong V (2012) *Jack-up Reinstallation Near Existing Footprints*. PhD thesis, University of Western Australia, Crawley, Australia.

Martin, C and Randolph, M (2006) Upper-bound analysis of lateral pile capacity in cohesive soil. Géotechnique, 56(2), 141-145.

Morton JP, O'Loughlin CD, and White DJ (2014) Strength assessment during shallow penetration of a sphere in clay. *Géotechnique Letters* **4**(1st October 2014): 262 – 266, http://dx.doi.org/10.1680/geolett.14.00049.

O'Loughlin C (2015) Session report: offshore geotechnics at ICPMG 2014. *International Journal of Physical Modelling in Geotechnics* **15(2)**: 98–115, http://dx.doi.org/10.1680/ijpmg.14.00040.

Punrattanasin P, Nishioka H, Murata O and Kusakabe O (2003) Development of combined loading apparatus for centrifuge test. *International Journal of Physical Modelling in Geotechnics* **3(4)**: 1–13.

Randolph MF (2012) Offshore geotechnics – the challenges of deepwater soft sediments. In *Geotechnical Engineering State of the Art and Practice: Keynote Lectures from GeoCongress 2012* (Rollins K and Zekkos D (eds)). American Society of Civil Engineers, Reston, VA, USA, Geotechnical Special Publication no. 226, pp. 241–271.

Randolph MF and Hope S (2004) Effect of cone velocity on cone resistance and excess pore pressures. In *Proc. Int. Sym. on Eng. Practice and Performance of Soft Deposits*. Osaka, Japan, pp. 147–152.

Randolph MF, Gaudin C, Gourvenec SM et al. (2011) Recent advances in offshore geotechnics for deep water oil and gas developments. *Ocean Engineering* **38(7)**: 818–834, http://dx.doi.org/10.1016/j.oceaneng.2010.10.021.

Randolph MF, Jewell RJ, Stone KJ, and Brown TA (1991) Establishing a new centrifuge facility. In *Proc. Int. Conf. on Centrifuge Modelling, Centrifuge '91, Boulder* (Ko H-Y, and McLean FG (eds)). Balkema, Rotterdam, Netherlands, pp. 3–9.

Stewart DP and Randolph MF (1991) A new site investigation tool for the centrifuge. In *Proceedings of Int. Conf. on Centrifuge Modelling, Centrifuge '91, Boulder* (Ko H-Y, and McLean FG (eds)). Balkema, Rotterdam, Netherlands, pp. 531–538.

Zhang Y, Bienen B and Cassidy MJ (2013) Development of a combined VHM loading apparatus for a geotechnical drum centrifuge. *International Journal of Physical Modelling in Geotechnics* **13(1)**: 13–90, http://dx.doi.org/10.1680/ijpmg.12.00007.

9. LIST OF FIGURES

Figure 1. Schematic of loading arm and actuator system highlighting: (a) movement in the vertical direction, (b) movement in the horizontal direction, (c) loading arm profile view in the *y-z* plane, and (d) loading arm profile view in the *x-z* plane.

Figure 2. Positive sign convention for loads and displacements acting on a rectangular foundation.

Figure 3. Undrained shear strength profile with depth of soil model derived from a T-bar penetrometer test.

Figure 4. Model foundation: (a) schematic drawing along the long side (y-z plane), and (b) schematic drawing along the short side (x-z plane).

Figure 5. Schematic of the loading arm and model foundation movements through: (a) vertical motion of the loading actuator, (b) horizontal motion of the loading actuator, (c) rotation about x-axis of the foundation at the foundation hinge, and (d) rotation about y-axis of the foundation through the horizontal roller bearing.

Figure 6. Centrifuge tests loading program showing time-scales of the (a) vertical load, V and (b) horizontal displacement, u_y imposed on the mudmat foundation.

Figure 7. Time-scale plots of the vertical load (V), horizontal displacement (u_y), horizontal load (H), vertical displacement ($w_{(laser)}$), and foundation rotation about the x and y axes (θ_{xx} and θ_{yy}) during: (a-e) touchdown of the foundation into the soil surface, (f-j) post-installation consolidation and undrained sliding cycles, and (k-o) first sliding and reconsolidation cycle.

Figure 8. Improved load control by reducing mechanical backlash.

Figure 9. Comparison of foundation movements as measured by the actuator encoders, and independently by lasers in (a) vertical, and (b) horizontal direction.

Figure 10. Complete set of test showing: (a) foundation settlement (laser), $w_{(laser)}$ and (b) horizontal load, H plotted against horizontal displacement (encoder), $u_{y(encoder)}$, and mid-slide values of (c) foundation settlement (laser), $w_{(laser)}$, (d) horizontal load, H, and (e) rotation about the x and y axes, θ_{xx} and θ_{yy} plotted against cycle number, N.

Figure 11. (a) Post-touchdown and cyclic consolidation settlement plotted against cycle number, N (inset: void ratio profile with depth obtained at a free-field soil (virgin), e_0 and within foundation footprint soil), and (b) overview photograph of foundation footprint after the test, showing peripheral berm formation.

Figure 12. Coefficient of sliding friction, $\mu = H/V$ (a) during the first slide and (b) during the loading cycles plotted against normalised horizontal displacement (encoder), $u_{y(encoder)}/B$, and (c) mid-slide values plotted against cycle number, N.

Figure 1. Schematic of loading arm and actuator system highlighting: (a) movement in the vertical direction, (b) movement in the horizontal direction, (c) loading arm profile view in the *y*-*z* plane, and (d) loading arm profile view in the *x*-*z* plane.

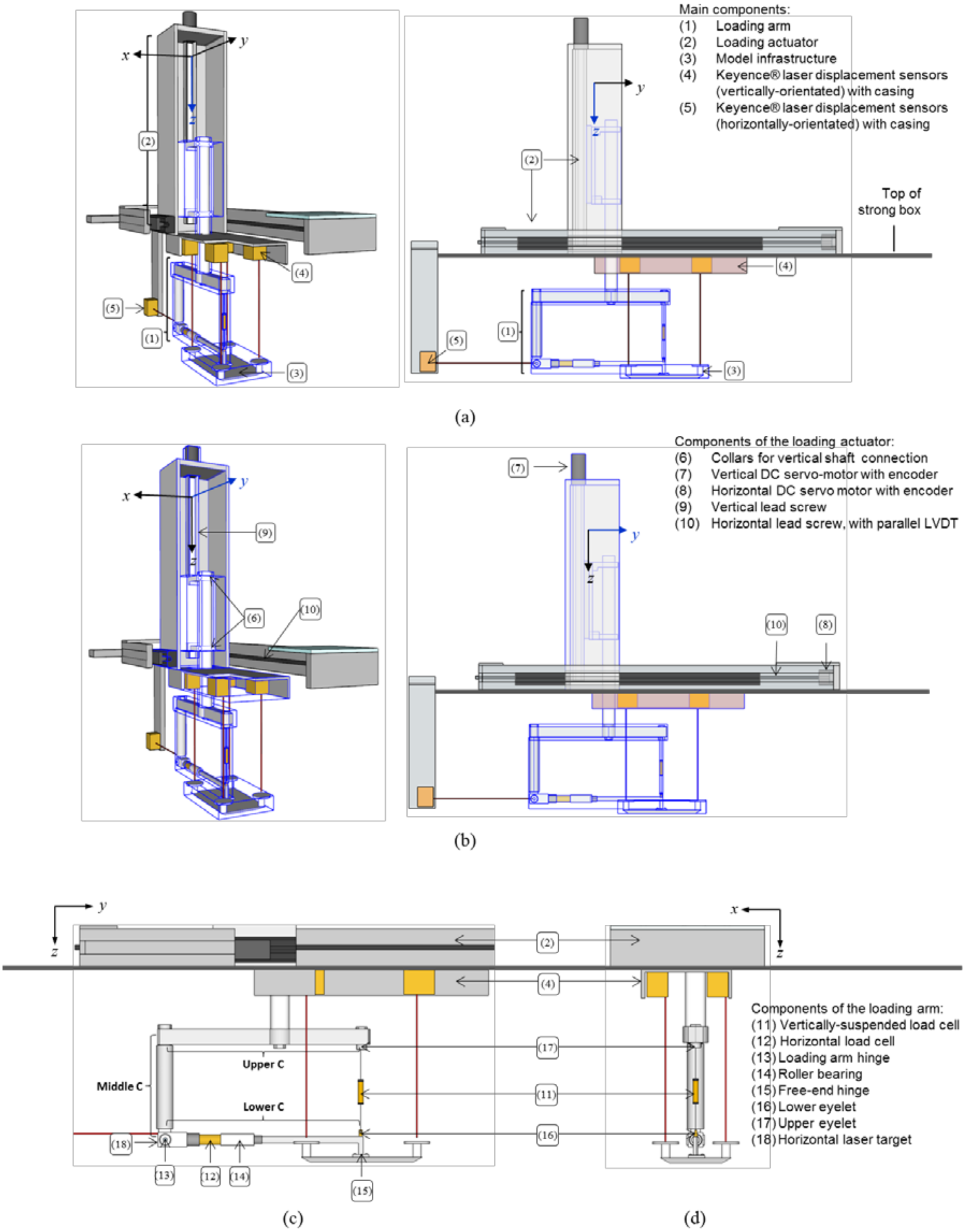

Figure 2. Positive sign convention for loads and displacements acting on a rectangular foundation.

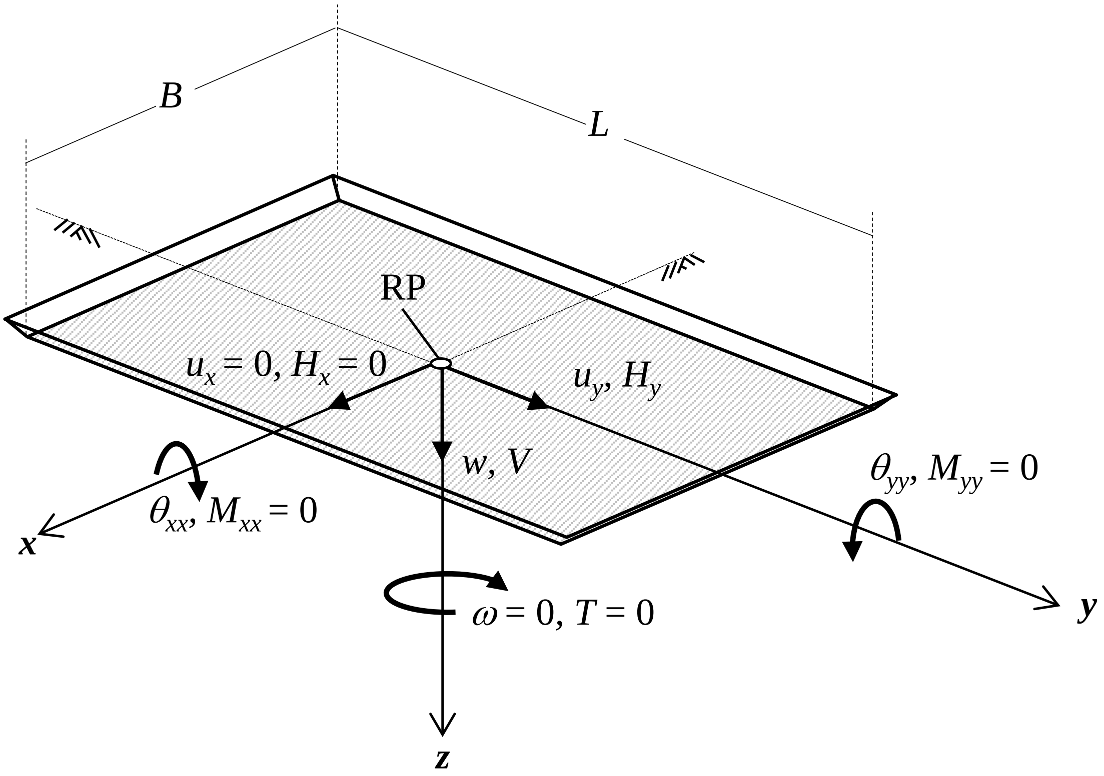

Figure 3. Undrained shear strength profile with depth of soil model derived from a T-bar penetrometer test.

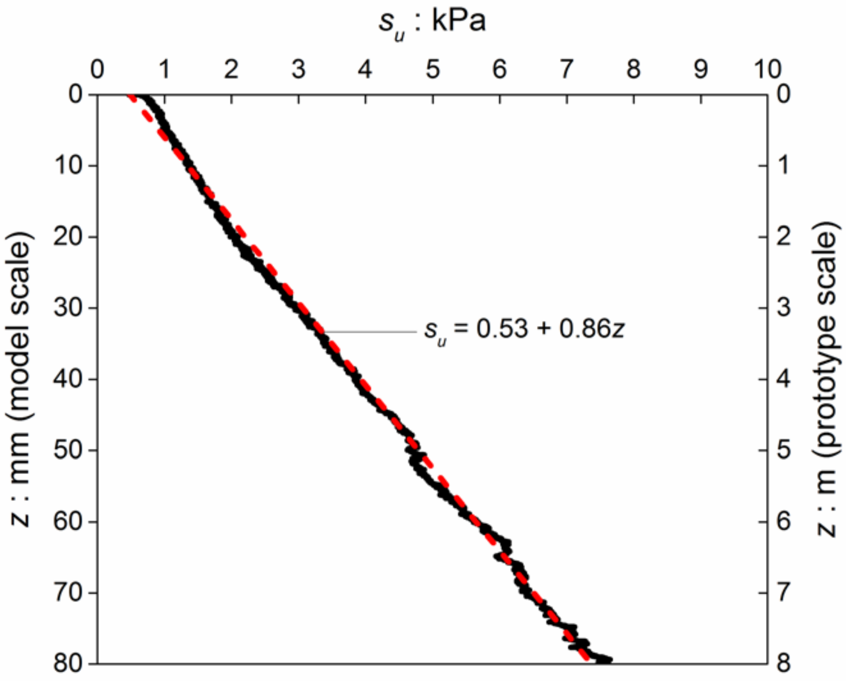

Figure 4. Model foundation: (a) schematic drawing along the long side (*y*-*z* plane), and (b) schematic drawing along the short side (*x*-*z* plane)

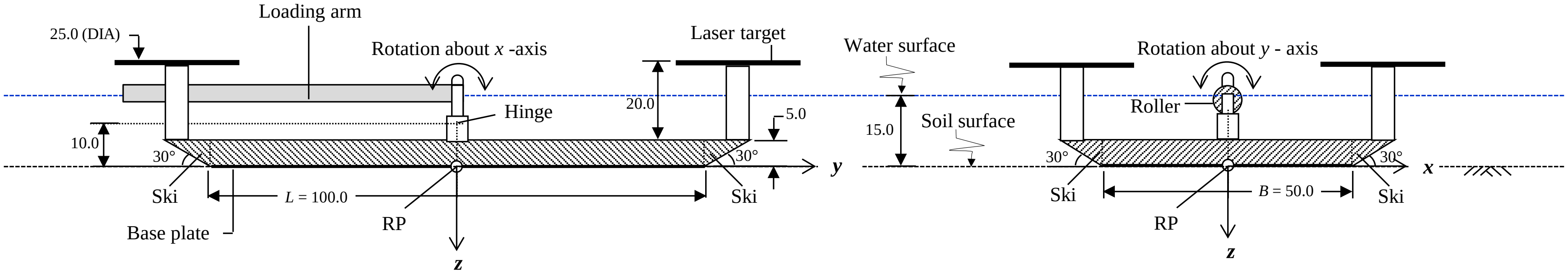

(a) (b)

Figure 5. Schematic of the loading arm and model foundation movements through: (a) vertical motion of the loading actuator, (b) horizontal motion of the loading actuator, (c) rotation about *x*-axis of the foundation at the foundation hinge, and (d) rotation about *y*-axis of the foundation through the horizontal roller bearing.

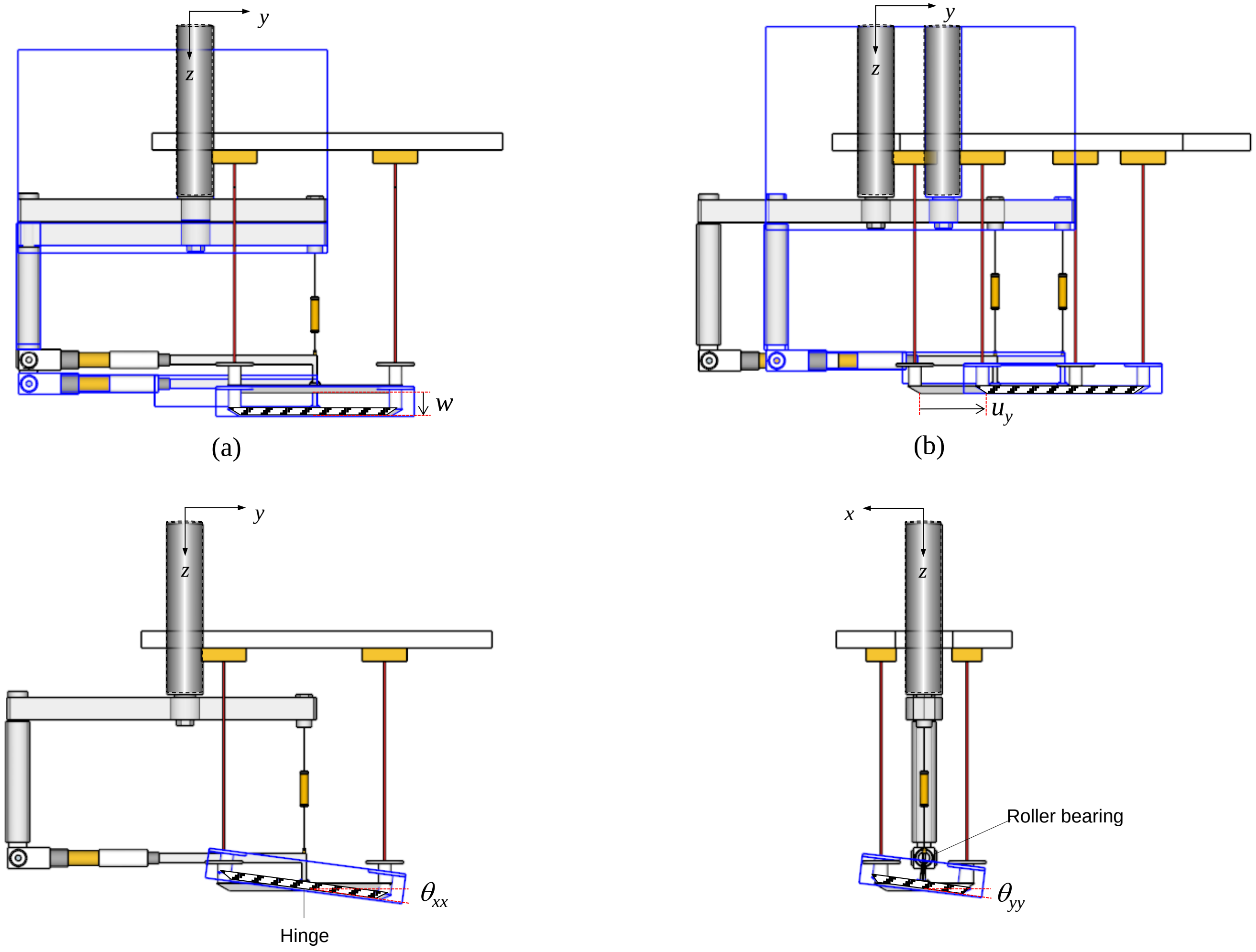

(a) (b) (c) (d)

Figure 6. Centrifuge tests loading program showing time-scales of the (a) vertical load, V and (b) horizontal displacement, u_y imposed on the mudmat foundation.

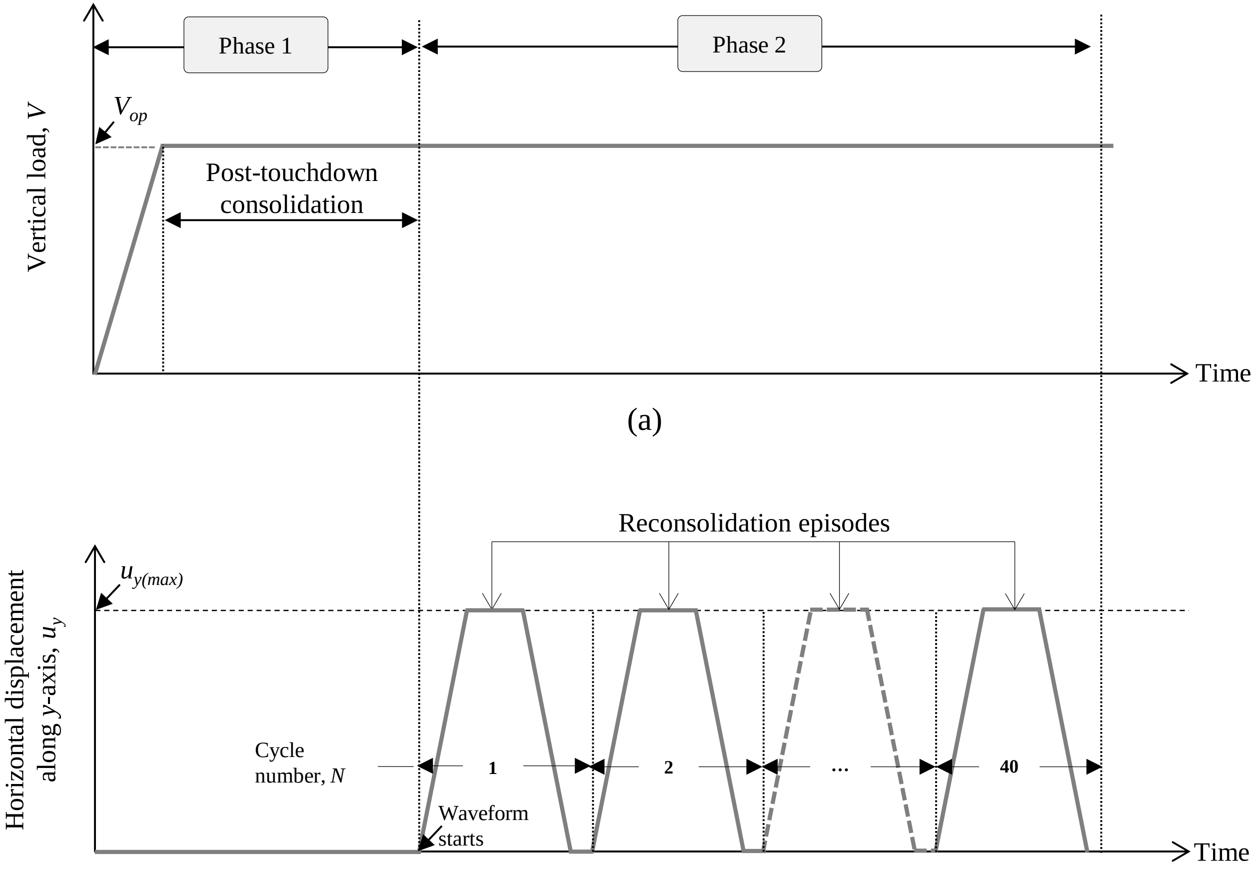

(a)

(b)

Figure 7. Time-scale plots of the vertical load (V), horizontal displacement (u_y), horizontal load (H), vertical displacement ($w_{(laser)}$), and foundation rotation about the x and y axes (θ_{xx} and θ_{yy}) during: (a-e) touchdown of the foundation into the soil surface, (f-j) post-installation consolidation and undrained sliding cycles, and (k-o) first sliding and reconsolidation cycle

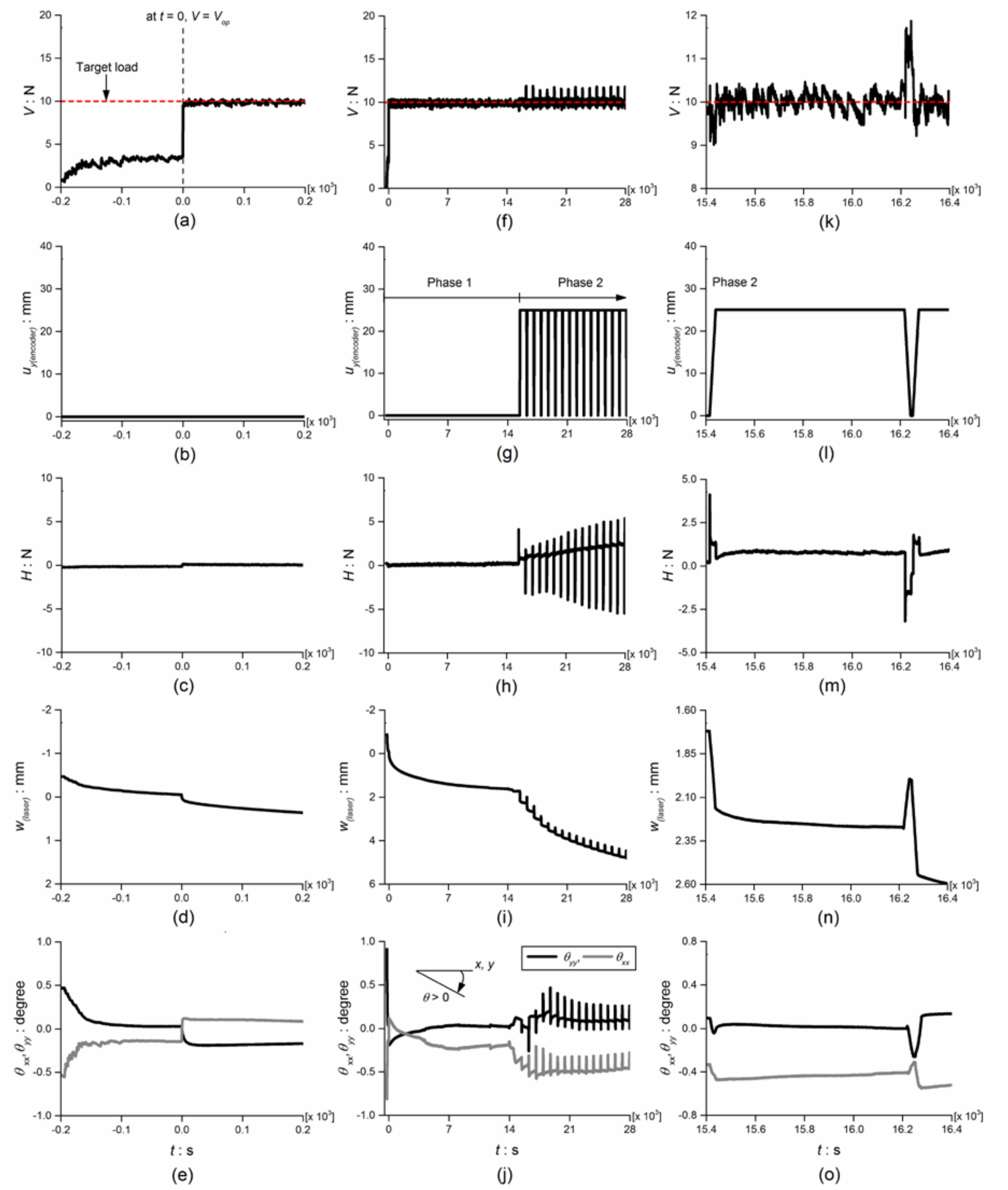

Figure 8. Improved load control by reducing mechanical backlash.

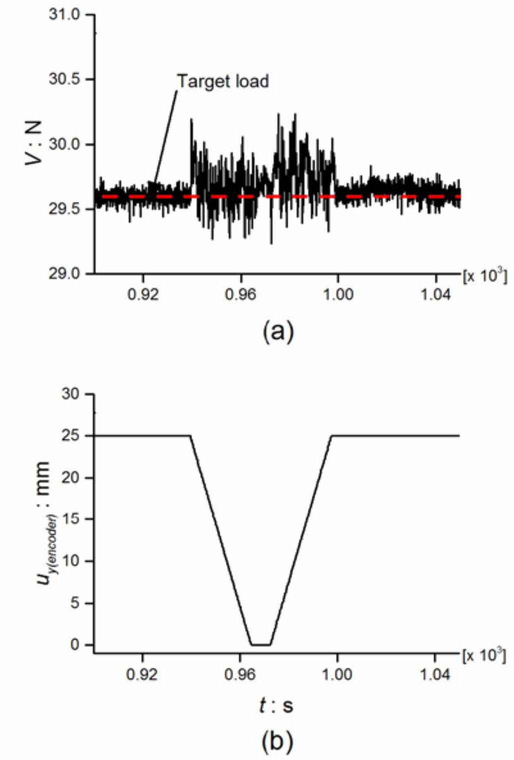

Figure 9. Comparison of foundation movements as measured by the actuator encoders, and independently by lasers in (a) vertical, and (b) horizontal direction.

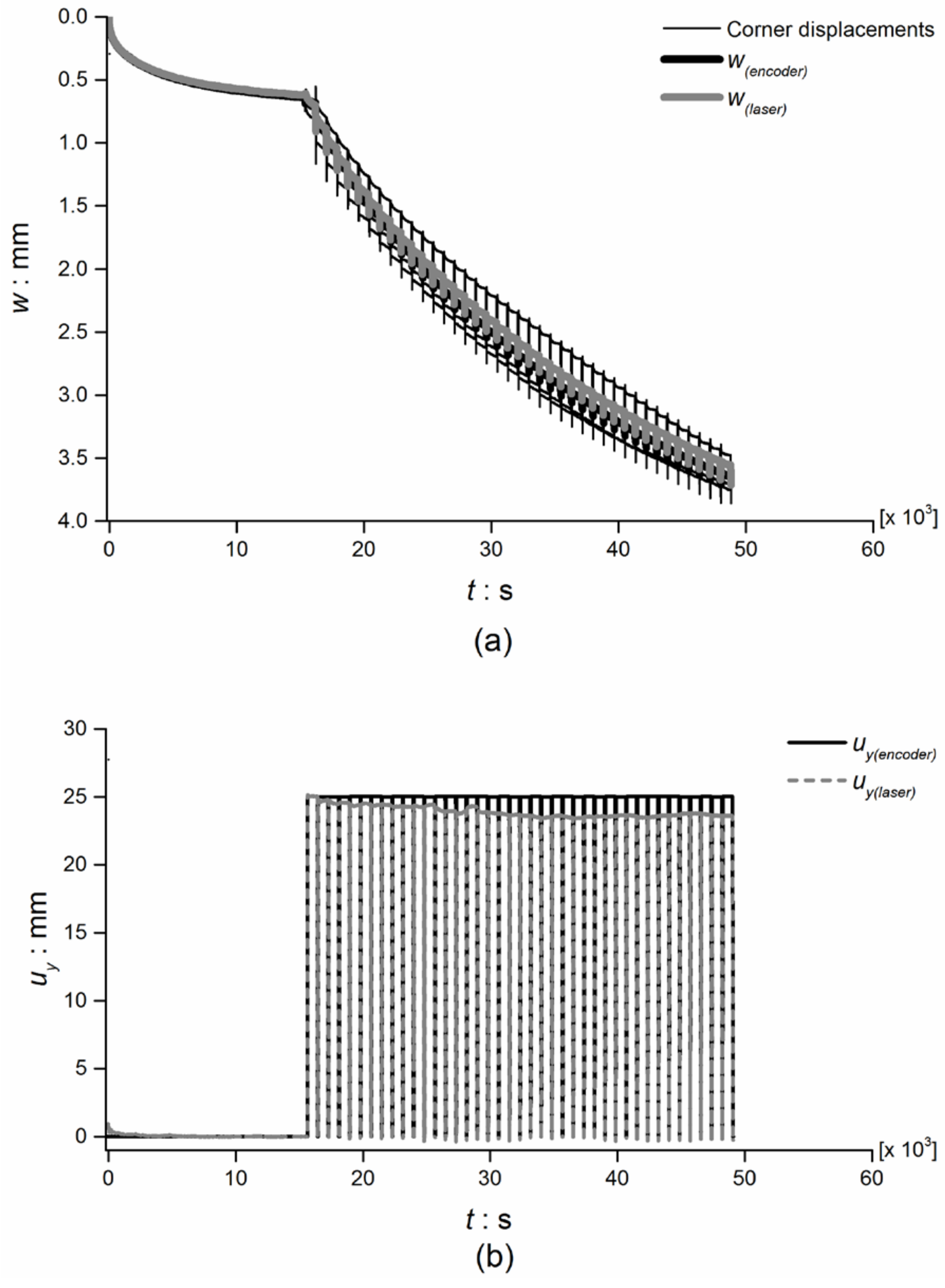

Figure 10. Complete set of test showing: (a) foundation settlement (laser), $w_{(laser)}$ and (b) horizontal load, H plotted against horizontal displacement (encoder), $u_{y(encoder)}$, and mid-slide values of (c) foundation settlement (laser), $w_{(laser)}$, (d) horizontal load, H, and (e) rotation about the x and y axes, θ_{xx} and θ_{yy} plotted against cycle number, N.

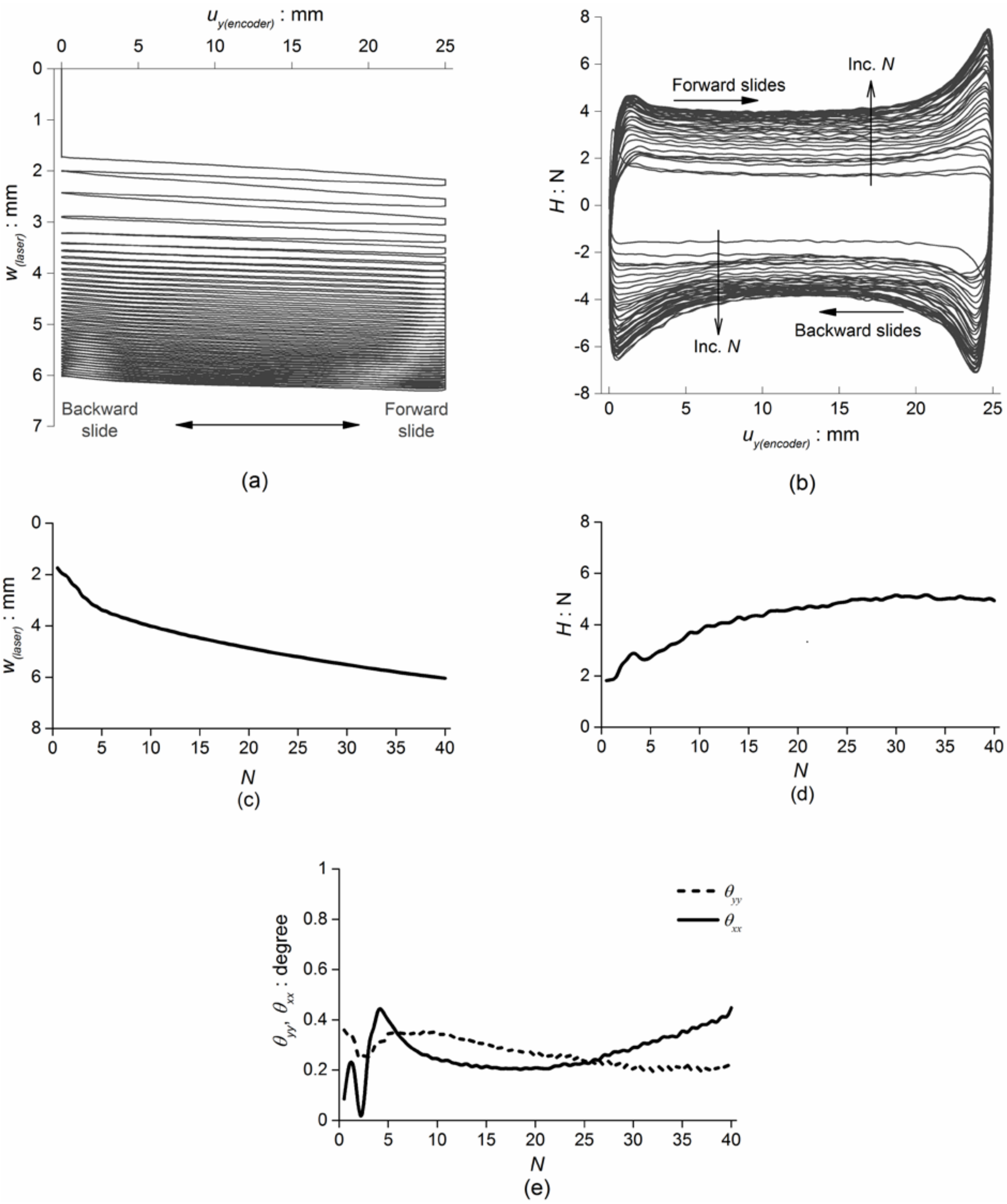

Figure 11. (a) Post-touchdown and cyclic consolidation settlement plotted against cycle number, *N* (inset: void ratio profile with depth obtained at a free-field soil (virgin), e_0 and within foundation footprint soil), and (b) overview photograph of foundation footprint after the test, showing peripheral berm formation.

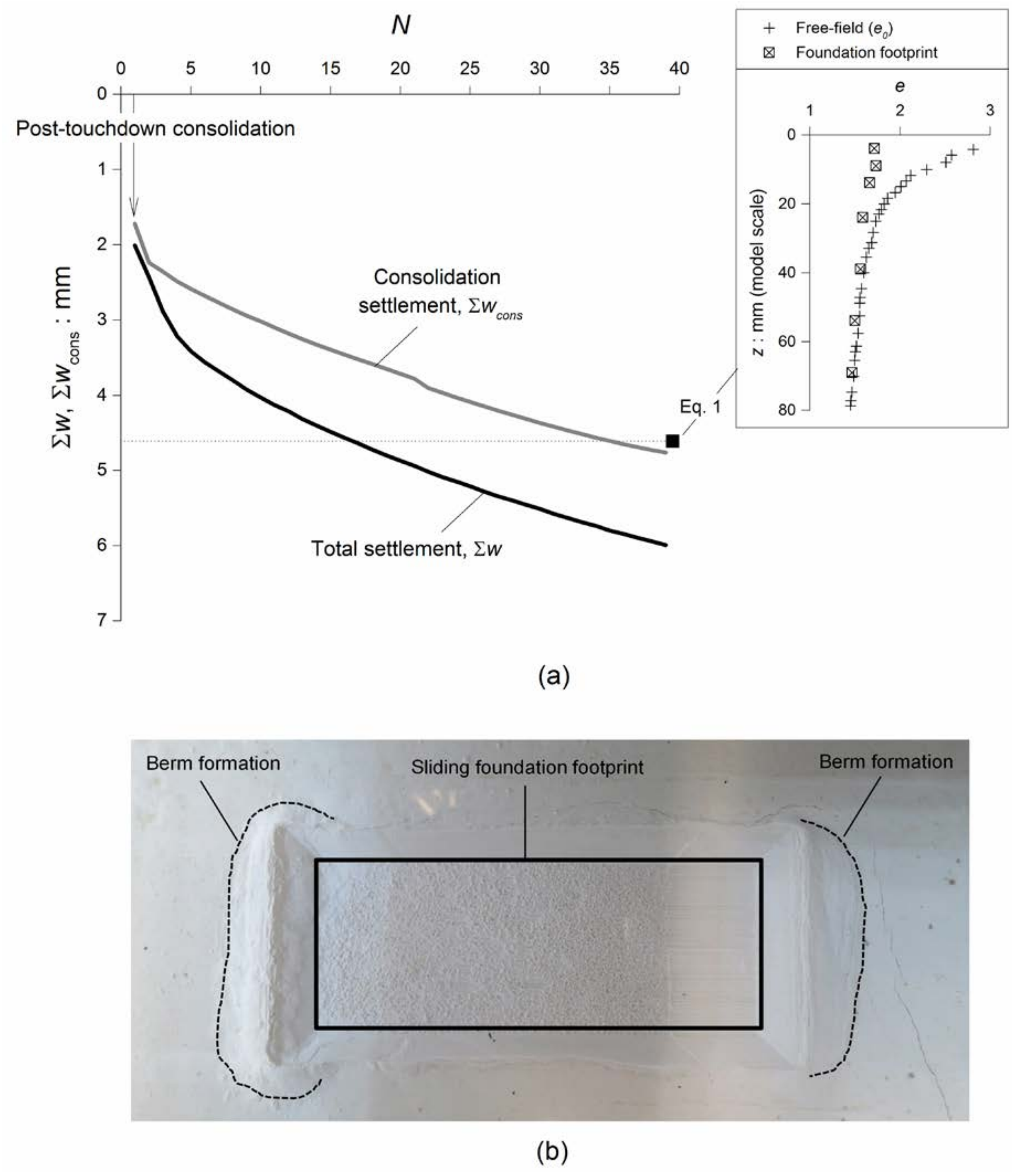

Figure 12. Coefficient of sliding friction, $\mu = H/V$ (a) during the first slide and (b) during the loading cycles plotted against normalised horizontal displacement (encoder), $u_{y(encoder)}/B$, and (c) mid-slide values plotted against cycle number, N.